

September 17, 2001

hep-th/0008245

US-00-07

# Wall and Anti-Wall in the Randall-Sundrum Model and A New Infrared Regularization

Shoichi ICHINOSE <sup>1</sup>

Laboratory of Physics,  
School of Food and Nutritional Sciences,  
University of Shizuoka, Yada 52-1, Shizuoka 422-8526, Japan

## Abstract

An approach to find the field equation solution of the Randall-Sundrum model with the  $S^1/Z_2$  extra axis is presented. We closely examine the infrared singularity. The vacuum is set by the 5 dimensional Higgs field. Both the domain-wall and the anti-domain-wall naturally appear, at the *ends* of the extra compact axis, by taking a *new infrared regularization*. The stability is guaranteed from the outset by the kink boundary condition. A *continuous* (infrared-)regularized solution, which is a truncated *Fourier series* of a *discontinuous* solution, is utilized. The ultraviolet-infrared relation appears in the regularized solution.

PACS NO: 04.25.-g, 04.50.+h, 11.10.Kk, 11.25.Mj, 11.27.+d, 12.10.Kt

Key Words: Randall-Sundrum model, Compactification, Extra dimension, Domain Wall, Regularization, Fourier Series

---

<sup>1</sup> E-mail address: ichinose@u-shizuoka-ken.ac.jp

# 1 Introduction

As an approach to explain the mass hierarchy problem, the Randall-Sundrum (RS) model[1, 2] have been taking people's attention both from the phenomenology[3] and from the theory[4, 5]. The model has, in fact, some advantages compared with other approaches such as the Kaluza-Klein compactification [6, 7] and the (standard) renormalization group approach . The most characteristic point is its exponential damping factor (warp factor) which could have the possibility of naturally explaining the broadly-spreading mass hierarchy ranging from the cosmological constant ( $10^{-41}$  GeV), through the weak physics ( $10^2$  GeV), to the Planck mass ( $10^{19}$  GeV). Furthermore the recent progress in the AdS/CFT correspondence[8, 9, 10] indicates the RS-model solution, which is a *classical* solution in the 5 dim AdS space-time, could be regarded as the renormalization trajectory in the 4 dim *quantum* solution.

We point out, however, an incomplete aspect in most approaches so far. They assume the  $\delta$ -function or  $\theta$ -function distribution from the outset as a form of the classical solution in order to make a ("infinitely-thin") wall configuration. Indeed it gives an easy "tool" to analyse the model in some limited situation. It is, however, obscure from the standpoint of the soliton (kink) physics and does miss the important role of the "thickness" in the regularization standpoint. The configuration, considered in the RS-model, generally has a domain wall structure with some *finite* thickness which is determined by the vacua in the asymptotic regions (or the boundary conditions) and some parameters in the system. In some limited configuration, the thickness approaches zero and the  $\delta$ -function (or  $\theta$ -function) appears as a well-regularized object. In such a way, we can understand the real meaning of the limit from the vacuum structure or the system parameters. This looks very important especially to understand the problem of the cosmological constant, which is the vacuum energy of the space-time. Needless to say, the system configuration should be derived by solving the field equation in a proper way. In some reference[11], the thickness was introduced just by smearing the assumed  $\delta$ -function. Such approach loses the real role of the thickness.

Motivated by the above things, a solution of the RS-model, for the one-wall case, has been presented [12, 13]. The points are 1) the wall configuration is obtained as a kink solution of the classical field equation of the 5 dim AdS gravity; 2) the  $\delta$ -function limit is specified by some parameters; 3) the vacua (asymptotic states), which are necessary to specify the kink, are

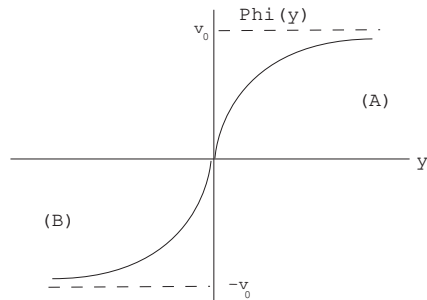


Fig.1 The scalar field for one-wall configuration [12].  $y \in \mathbf{R} = (-\infty, \infty)$ .

introduced by the 5 dim bulk Higgs potential; 4) the stability of the solution is guaranteed by the boundary condition. The obtained solution correctly gives the basic physical outputs such as the 4D Planck mass ( $M_{pl} \sim \sqrt{M^3/k}$ ) and the 4D cosmological constant ( $\Lambda_{4d} \sim -M^3k$ ) in terms of the 5D Planck mass ( $M$ ) and the thickness parameter ( $k$ ). These properties remain valid in the present case because we modify (with much care) only the infrared boundary condition. The configuration of a wall and an anti-wall is taken in the original work[1], but it is now considered unstable. To cure it, one approach is to take into account the radion field[14]. Here we point out another possibility of creating the wall-anti-wall configuration by taking a new infrared treatment which mimics the lattice situation.

It is well-known that the massless chiral fermion appears as a zero mode bound to the domain wall. Now we recall the similar situation takes place in the lattice field theory using the 5D lattice[15, 16]. In that case, besides the fact that the formulation is discrete, some essential differences are there. That is, the extra axis  $y$  is regularized to be *finite*  $-L \leq y \leq +L$  and the boundary condition for the extra axis is taken to be *periodic*:  $y \rightarrow y + 2L$ . In this case a wall appears at  $y = 0$  and an anti-wall appears at  $y = L$ . For every zero mode at  $y = 0$ , there is a zero mode of the opposite chirality at  $y = L$ . Every mode is *chirally paired*, which shows the *vector-like* nature of the 5D theory. The chiral anomaly in the 4D theory is now understood as the flow of the current through the fifth space[17]. In the lattice numerical simulation, this configuration is basically taken, with some improvements [18, 19, 20], and several physical quantities of QCD such as the pion mass are numerically calculated[21]. In order to realize the similar situation in the Randall-Sundrum model, we need the wall-anti-wall

configuration. We present a way to make the configuration from the one-wall solution of Ref.[12].

A focus here is to clarify some controversial point, that is, whether  $S^1/Z_2$  compactification of the kink configuration(Fig.1) is compatible with the wall-anti-wall configuration. On the one hand,  $S^1$  property requires the solution to be periodic with some finite periodicity in an extra axis. On the other, naive expectation implies its behavior, in an asymptotic region (A), does *not continuously* connect with that in (B) of their adjacent period, as far as (A) and (B) are *different vacua* which is required for the soliton (kink) configuration. Clearly this is related to the boundary and stability problems. The stability is guaranteed by the kink property: the two vacua (A) and (B) are related by the discrete (discontinuous) symmetry,  $\Phi \leftrightarrow -\Phi$ . To solve these problems, some close *infrared* treatment is necessary. Note that physical behaviors in both regions (A) and (B) are the same. (Both have the same 5D scalar Riemann curvature.) Further note that we do *not* consider a new solution of the kink-anti-kink type. We will first choose a correct coordinate where the wall-anti-wall configuration should appear and then *change* the infrared boundary condition for the one-wall solution previously obtained. We will show the new boundary condition gives us the other (anti-) wall. The present claim is that the (stable) wall-anti-wall solution exists by taking the correct coordinate and the *new infrared regularization* proposed here.

The present model of 5D gravity-scalar system is introduced in Sec.2. In Sec.3 we change the extra coordinate from the infinite one  $y \in \mathbf{R} = (-\infty, \infty)$  to a compact one  $z \in (-\frac{1}{2}r_c, +\frac{1}{2}r_c)$  in order to obtain the "size" of the extra space  $r_c$ . In Sec.4, by imposing the periodic boundary condition, we extend the coordinate region of  $z$  to  $\mathbf{R}$ . The new infrared regularization is explained in Sec.5, where the Fourier expansion of (continuous and discontinuous) periodic functions is exploited. Truncation of the infinitely expanded terms to the finite ones is the key of the present regularization. In Sec.6, we present the numerical solutions of the present model, and using this result, we fix all Fourier expansion coefficients numerically. We conclude and discuss in Sec.7. Some appendices are in order to supplement the text. In App.A, a compact coordinate, which is different from the one taken in the text, is examined. Some advantageous points are noticed. Numerical results of Sec.6 are explained in App.B. They consist of two standard method of the numerical calculus: the Runge-Kutta method and the Least Square method. In App.C, some simple function, which imitates the solution of the present model, is examined in order to clarify the characteristic properties of the

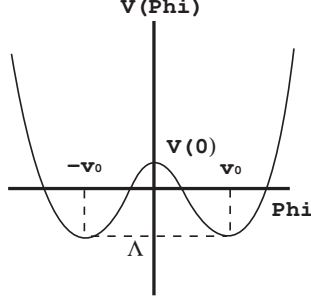


Fig.2 The Higgs Potential  $V(\Phi)$ , (1). Horizontal axis:  $\Phi$ . From (21),  
 $V(0) = \lambda v_0^4/4 + \Lambda > 0$ ,  $V(v_0) = \Lambda < 0$ .

Fourier expansion coefficients.

## 2 Model Set-Up

We take the following 5D gravitational theory with 5D Higgs potential.

$$S[G_{AB}, \Phi] = \int d^5 X \sqrt{-G} \left( -\frac{1}{2} M^3 \hat{R} - \frac{1}{2} G^{AB} \partial_A \Phi \partial_B \Phi - V(\Phi) \right) ,$$

$$V(\Phi) = \frac{\lambda}{4} (\Phi^2 - v_0^2)^2 + \Lambda \quad , \quad (1)$$

where  $X^A$  ( $A = 0, 1, 2, 3, 4$ ) is the 5D coordinates and we also use the notation  $(X^A) \equiv (x^\mu, y)$ ,  $\mu = 0, 1, 2, 3$ . The coordinate  $X^4 = y$  is the extra axis which is taken to be a space coordinate.  $\Phi$  is a 5D scalar field,  $G = \det G_{AB}$ ,  $\hat{R}$  is the 5D Riemannian scalar curvature.  $M(> 0)$  is the 5D Planck mass and is regarded as the *fundamental scale* of this dimensional reduction scenario.  $V(\Phi)$  is the Higgs potential and serves for preparing the (classical) vacuum in 5D world. The three parameters  $\lambda, v_0$  and  $\Lambda$  in  $V(\Phi)$  are called here *vacuum parameters*.  $\lambda(> 0)$  is a coupling,  $v_0(> 0)$  is the Higgs field vacuum expectation value, and  $\Lambda$  is the 5D cosmological constant. See Fig.2. It is later shown that the sign of  $\Lambda$  must be negative for the present domain wall configuration. The Einstein equation is given by

$$M^3 (\hat{R}_{MN} - \frac{1}{2} G_{MN} \hat{R}) = -\partial_M \Phi \partial_N \Phi + G_{MN} \left( \frac{1}{2} G^{KL} \partial_K \Phi \partial_L \Phi + V(\Phi) \right) ,$$

$$\nabla^2 \Phi = \frac{\delta V}{\delta \Phi} \quad . \quad (2)$$

Following Callan and Harvey[17], we consider the case that  $\Phi$  depends only on the extra coordinate  $y$ :  $\Phi = \Phi(y)$ . Because  $M$ -dependence can be absorbed by a simple scaling ( $\Phi = M^{3/2}\tilde{\Phi}$ ,  $v_0 = M^{3/2}\tilde{v}_0$ ,  $\lambda = M^{-1}\tilde{\lambda}$ ,  $\Lambda = M^5\tilde{\Lambda}$ ,  $X^A = M^{-1}\tilde{X}^A$ ), we may, for simplicity, take

$$M = 1 \quad . \quad (3)$$

We explicitly write  $M$  only when it is necessary.

### 3 Infinite Extra Axis and Its Compactification

We start with the following 5D metric[2, 12].

$$ds^2 = e^{-2\sigma(y)}\eta_{\mu\nu}dx^\mu dx^\nu + dy^2 \quad , \quad y \in \mathbf{R} = (-\infty, +\infty) \quad (4)$$

where  $\eta_{\mu\nu} = \text{diag}(-1, 1, 1, 1)$ . In this choice, the 4D Poincaré invariance is preserved. The Weyl factor  $e^{-2\sigma(y)}$  is called "warp factor" and is determined by the 5D Einstein equation. The extra axis taken here is an infinite real line  $\mathbf{R} = (-\infty, +\infty)$ . The coordinates  $(X^A) = (x^\mu, y)$  give one wall configuration by taking the boundary condition:  $\Phi(y) \rightarrow \pm v_0$ ,  $y \rightarrow \pm\infty$  and there exists a family of exact solution [12]. Now let us move from the  $y$ -coordinate to another one  $z$ (See Fig.3).

$$\frac{Mz}{Mr_c} = \frac{z}{r_c} = \frac{1}{2} \tanh(My) \quad , \quad \frac{z}{r_c} \in \left(-\frac{1}{2}, \frac{1}{2}\right) \quad , \quad (5)$$

where a *free* parameter  $r_c$  is introduced as the *compactification size*. (Another compactification is examined in Appendix A.) In the "wall region"  $|y| \ll 1/M$  (or  $|z| \ll r_c$ ),  $z$ -coordinate and  $y$ -coordinate are almost same except a simple factor :  $z \approx y \times \frac{Mr_c}{2}$ . In the asymptotic (infrared) regions  $|y| \gg 1/M$  (or  $|z| \approx r_c/2$ ), they differ significantly :  $z/r_c \approx \pm(\frac{1}{2} - e^{-2M|y|})$  as  $My \rightarrow \pm\infty$ . Without confusion, we may take

$$r_c = 1 \quad . \quad (6)$$

(When  $r_c$ -dependence is required, it is easily obtained by the substitution  $z \rightarrow z/r_c$ . ) In terms of the new coordinate  $z$ , the line element (4) reduces to

$$ds^2 = e^{-2\sigma(z)}\eta_{\mu\nu}dx^\mu dx^\nu + \frac{4}{(1-4z^2)^2}dz^2 \quad , \quad dz = \frac{1}{2}(1-4z^2)dy \quad , \quad z \in \left(-\frac{1}{2}, \frac{1}{2}\right) \quad . \quad (7)$$

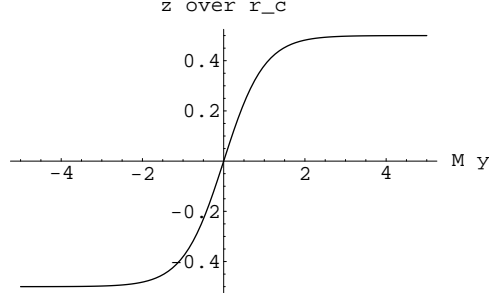


Fig.3 Relation between two coordinates,  $z$  (compact) and  $y$  (noncompact),  
(5). Vertical axis:  $\frac{z}{r_c}$ ; Horizontal axis:  $My$ .

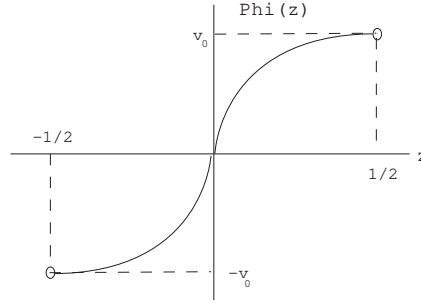


Fig.4 The Higgs field with the boundary condition (9). Vertical axis:  $\Phi(z)$ ;  
Horizontal axis:  $z$ .

$z = \pm \frac{1}{2}$  are the points of the *coordinate singularity*. The 5D Riemann scalar curvature is given by

$$\hat{R} = F(-2F\sigma'' + 5F\sigma'^2 - 2F'\sigma') \quad , \quad F \equiv 1 - 4z^2 \quad , \quad \sigma' = \frac{d\sigma}{dz} \quad , \quad (8)$$

and it turns out that there are *no curvature singularities anywhere*, for the solution we will consider. Let us consider the case the 5D Higgs field  $\Phi(z)$  has the following boundary condition(Fig.4).

$$\lim_{z \rightarrow \pm(\frac{1}{2}-0)} \Phi(z) \rightarrow \pm v_0 \quad , \quad v_0 > 0 \quad . \quad (9)$$

$\pm v_0$  is the vacuum expectation value in the asymptotic region  $z \rightarrow \pm(\frac{1}{2}-0)$ .

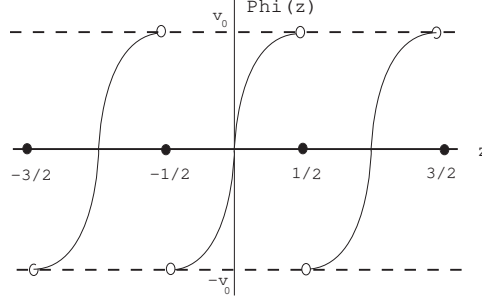


Fig.5 The periodically extended Higgs field  $\Phi(z)$ . Vertical axis:  $\Phi(z)$ ;  
Horizontal axis:  $z$ .

## 4 $S^1$ Extra Axis

In this section we move to the case where the extra axis is  $S^1$  through the following procedure. If we can properly regularize the coordinate singularity at  $z = \pm\frac{1}{2}$  in (7) (see the next section), the coordinate region  $-\frac{1}{2} \leq z \leq \frac{1}{2}$  can be extended to  $\mathbf{R} = (-\infty, \infty)$  as follows.

1. We require the periodic boundary condition :

$$\Phi(z) = \Phi(z+1) \quad , \quad \sigma(z) = \sigma(z+1) \quad (\text{or} \quad \sigma'(z) = \sigma'(z+1)) ; \quad (10)$$

2. Values of  $\Phi$  at  $z = \frac{1}{2} + \mathbf{Z}$  are *defined* as,

$$\Phi\left(\frac{1}{2} + \mathbf{Z}\right) \equiv 0 ; \quad (11)$$

3. The universal covering space is taken to be the real number space :

$$\left[-\frac{1}{2}, \frac{1}{2}\right] \times \mathbf{Z} = (-\infty, \infty) = \mathbf{R} ; \quad (12)$$

where  $\mathbf{Z} = \{0, \pm 1, \pm 2, \dots\}$ . See Fig.5 for the schematic behavior of  $\Phi(z)$ . Note that we have here *newly defined* the values of  $\Phi(z)$  at the singular points  $z = \frac{1}{2} + \mathbf{Z}$  (coordinate singularity, not the curvature singularity). The points correspond to  $y = \pm\infty$  of the original coordinate,  $y$ .  $\Phi(y = \pm\infty)$  are not defined in Sec.3. In (11) we have specified the present treatment of



$y = \pm\infty$ , and which should be regarded as a part of the present infrared regularization.<sup>2</sup> This specification turns out to be important in Sec.5.

We furthermore note that the translation invariance  $y \rightarrow y + c$  in (4) reduces to the periodicity invariance (discrete version of the translation)  $z \rightarrow z + 1$ . (The situation is the same as the lattice regularization of the continuum space.) The loss of the translation freedom  $c$  is traded with the freedom of the coordinate choice  $r_c$ .

$\Phi(z)$  defined above has the properties:

**P1** Piecewise continuous. (*Discontinuous* at  $z = \frac{1}{2} + \mathbf{Z}$ .)

**P2** Piecewise smooth. ( $\Phi'(z)$  is piecewise continuous.)

**P3** Periodic ( $S^1$ -symmetry) :  $z \rightarrow z + 1$ .

**P4** Odd function of  $z$  ( $Z_2$ -symmetry) :  $\Phi(z) = -\Phi(-z)$ .

We call these "Φ-properties".

At present, except for the coordinate-singularity points  $z = \frac{1}{2} + \mathbf{Z}$ , the metric (7) is defined for  $z \in \mathbf{R} = (-\infty, \infty)$ :

$$(G_{MN}) = \begin{pmatrix} e^{-2\sigma(z)}\eta_{\mu\nu} & 0 \\ 0 & \frac{4}{F(z)^2} \end{pmatrix}, \quad (13)$$

where  $F(z) = 1 - 4z^2$  at this stage (soon redefined) and  $M = (\mu, z)$ . The Einstein equation (2) reduces to the following two coupled differential equations for  $\Phi(z)$  and  $\sigma(z)$ .

$$\begin{aligned} -\frac{3}{2}\sigma'^2 F(z)^2 &= -\frac{1}{8}F(z)^2\Phi'^2 + V, \\ \frac{3}{4}\frac{1}{F(z)}(\sigma'F(z))' &= \frac{1}{4}\Phi'^2, \end{aligned} \quad (14)$$

where  $\sigma' = \frac{d\sigma}{dz}$ ,  $\Phi' = \frac{d\Phi}{dz}$ . In order to make the above equations periodic in  $z$  :  $z \rightarrow z + 1$ , we must replace  $F(z) = 1 - 4z^2$  by its "periodic generalization"<sup>3</sup> :

$$F(z) = \begin{cases} 1 - 4z^2 & \text{for } -\frac{1}{2} \leq z \leq \frac{1}{2} \\ 1 - 4z'^2 & \text{for } |z| > \frac{1}{2} \\ (z = z' + n, -\frac{1}{2} \leq z' \leq \frac{1}{2}, n = \pm 1, \pm 2, \dots) \end{cases}$$

---

<sup>2</sup> This procedure reminds us of the similar one in the case of making the sphere topology (compact) from the  $\mathbf{E}^2$  space (non-compact) by introducing the point of infinity.

<sup>3</sup> When we take another compact coordinate  $w$ , defined in (49), this "periodic generalization" is not necessary.

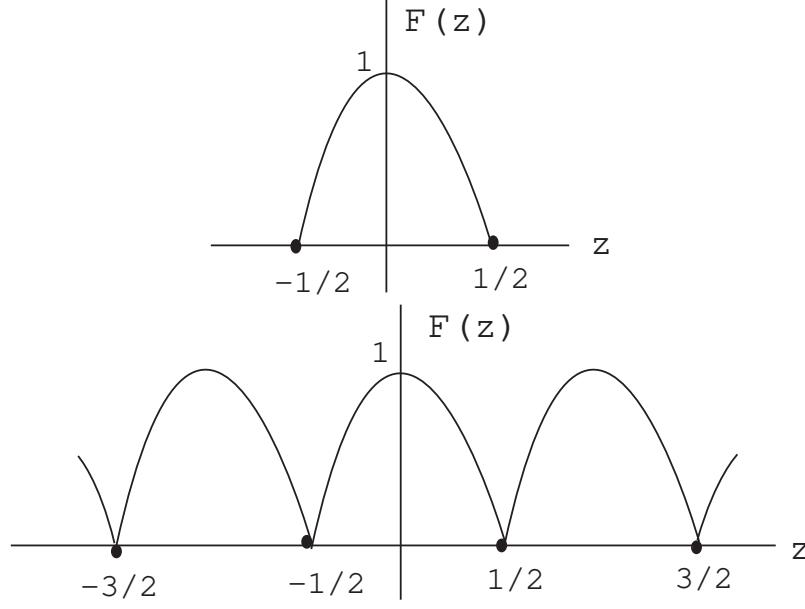


Fig.6 [Above] The function  $1 - 4z^2$  ( $-1/2 \leq z \leq 1/2$ ); [Below] The periodically generalized function  $[1 - 4z^2]$ , (15). Horizontal axis:  $z$ .

$$\equiv [1 - 4z^2] \quad , \quad (15)$$

See . We denote the periodically generalization of a function  $f(x)$  as  $[f(x)]$ . From the definition,  $F(z) = [1 - 4z^2]$  has the following properties.

**F1** Continuous function of  $z$ .

**F2** Piecewise smooth ( $F'(z)$  is singular at  $z = \frac{1}{2} + \mathbf{Z}$ ).

**F3** Periodic ( $S^1$ -symmetry) :  $F(z) = F(z + 1)$ .

**F4** Even function of  $z$  ( $Z_2$ -symmetry) :  $F(z) = F(-z)$ .

**F5** Positive semi-definiteness :  $F(z) \geq 0$ .

We call these properties "F-properties". This process of replacing  $(1 - 4z^2)$  by  $[1 - 4z^2]$  of (15) should be regarded as a part of the present (infrared) regularization.

For some later use, we present here the *Fourier expansion* of  $F(z)$ .

$$F(z) = \frac{2}{3} + \frac{4}{\pi^2} \sum_{l=1}^{\infty} \frac{(-1)^{l+1}}{l^2} \cos(2\pi lz) \quad . \quad (16)$$

This expression can be taken as the definition of  $F(z)$  instead of (15).

We can fix the asymptotic form of  $\sigma'(z)$  using (14) as follows. In this process of "periodic generalization", the boundary condition (9) is also generalized to be

$$\lim_{z \rightarrow \pm(\frac{1}{2}-0)+\mathbf{Z}} \Phi(z) = \pm v_0 \quad , \quad v_0 > 0 \quad . \quad (17)$$

(Note  $\Phi(\pm\frac{1}{2}+\mathbf{Z}) = 0$  as introduced in (11).) We call the asymptotic regions  $\{z|z \rightarrow \pm(\frac{1}{2}-0)+\mathbf{Z}\}$  IR-regions and another regions  $\{z|z \rightarrow \pm 0+\mathbf{Z}\}$  UV-regions. In the IR-regions,  $\Phi' \rightarrow 0$  from the above equation, therefore  $\sigma'F(z) \rightarrow \text{constant}$  from the second eq. of (14). Furthermore, using the first equation, we obtain

$$\lim_{z \rightarrow \pm(\frac{1}{2}-0)+\mathbf{Z}} \Sigma(z) = \pm\omega \quad , \quad \omega = \sqrt{-\frac{2\Lambda}{3}} \quad . \quad (18)$$

where  $\Sigma(z) \equiv F(z)\sigma'(z)$ . Note that  $\Sigma(z) = 2\frac{d\sigma}{dy}$  for  $-\frac{1}{2} \leq z \leq \frac{1}{2}$ . The behavior of the "warp" factor field  $\Sigma(z)$  will be shown to be similar to the Higgs field  $\Phi(z)$ . ( $\Phi(z)$  and  $\Sigma(z)$  will be parallelly discussed in Sec.5 and 6.) In eq.(18), we notice  $\Lambda$  should be negative :  $\Lambda \leq 0$ . From the first eq. of (14), we know

$$\frac{1}{8}F(z)^2\Phi'^2 = \frac{3}{2}\Sigma(z)^2 + V \geq 0 \quad . \quad (19)$$

From the field equations (14) and the boundary conditions (17,18), we conclude  $\Sigma(z)$  and  $\Phi(z)$  are *odd* functions of  $z$ . Hence we have

$$\Sigma(z) = 0 \quad \text{and} \quad \Phi(z) = 0 \quad \text{at} \quad z = 0 \quad . \quad (20)$$

(This condition will be used to solve the field equations (14) numerically. The boundary conditions (17,18) cannot be taken due to the singularity. See Appendix B.) Applying this result to (19), we know  $\frac{\lambda}{4}v_0^4 + \Lambda \geq 0$ . Combining the previous result, we obtain[12]

$$-\frac{\lambda}{4}v_0^4 \leq \Lambda \leq 0 \quad . \quad (21)$$

It says the sign of  $\Lambda$  should be negative (anti de Sitter) and the absolute value has the *upper* bound:  $|\Lambda| \leq \frac{\lambda}{4} v_0^4$ . Near the singular points,  $z \rightarrow \pm(\frac{1}{2} - 0)$ , the asymptotic behavior of the line element is given by, from (18),

$$ds^2 = \left| \frac{1+2z}{1-2z} \right|^{\mp\omega/2} \eta_{\mu\nu} dx^\mu dx^\nu + \frac{4}{(1-4z^2)^2} dz^2 \quad , \quad \omega = \sqrt{-\frac{2\Lambda}{3}} \quad , \quad (22)$$

which shows the singular points are horizons. The power-law of the Weyl factor ("warp factor") indicates the *scaling* behavior of the system when  $z \rightarrow \pm(\frac{1}{2} - 0)$ . See Sec.7.

## 5 Infrared Regularization at $z = \frac{1}{2} + \mathbf{Z}$

We come to the most important part of the present regularization. Before the presentation, we give here a mathematically well-known fact. The periodic step function  $\theta(x)$  defined by

$$\theta(x) = \begin{cases} 1 & 2n\epsilon < x < (2n+1)\epsilon \\ 0 & x = n\epsilon \\ -1 & (2n+1)\epsilon < x < (2n+2)\epsilon \end{cases} \quad , \quad (23)$$

where  $n \in \mathbf{Z}$  (see Fig.7). It has the following properties:

**T1** Piecewise continuous. (*Discontinuous* at  $x \in \epsilon \times \mathbf{Z}$ .)

**T2** Piecewise smooth.

**T3** Periodic ( $S^1$ -symmetry) :  $\theta(x + 2\epsilon) = \theta(x)$ .

**T4** Odd function of  $x$  ( $Z_2$ -symmetry) :  $\theta(x) = -\theta(-x)$ .

**T5** Symmetric with respect to the axes  $x = (\pm\frac{1}{2} + 2\mathbf{Z})\epsilon$  (UV-IR symmetry).

These are similar to  $\Phi$ -properties (for  $\epsilon = \frac{1}{2}$ ) except for Property T1 (the number of discontinuous points doubles) and Property T5 (UV-IR relation). We call these properties " $\theta$ -properties". The periodic step function  $\theta(x)$ , which is *discontinuous*, has the following Fourier expansion.

$$\theta(x) = \frac{4}{\pi} \sum_{l=0}^{\infty} \frac{1}{2l+1} \sin\left\{(2l+1)\pi \frac{x}{\epsilon}\right\} \quad . \quad (24)$$

(Compare the Fourier expansion of the *continuous* function  $F(z)$ , (16). Main changes are,  $2l$  in  $F(z)$  is replaced by  $(2l+1)/\epsilon = 2(2l+1)$  for  $\epsilon = 1/2$ ,

and the coefficient  $(-1)^{l+1}/l^2$  is by  $1/(2l+1)$ . The discontinuous case is less convergent series than the continuous case. ) When we *regularize* (24) by the *finite* ( $L$ ) sum,

$$\theta_L(x) = \frac{4}{\pi} \sum_{l=0}^L \frac{1}{2l+1} \sin\{(2l+1)\pi \frac{x}{\epsilon}\} \quad , \quad (25)$$

then  $\theta_L(x)$  has the following new properties compared with  $\theta(x)$ :

**TL1** *Continuous* everywhere  $x \in \mathbf{R} = (-\infty, \infty)$  (see Fig.5). Especially  $\theta_L(x \in \epsilon\mathbf{Z}) = 0$ .

**TL2** Smooth everywhere.

Other items 3,4 and 5 are the same as  $\theta(x)$ : **TL3=T3**, **TL4=T4**, **TL5=T5**. We call these properties " $\theta_L$ -properties". This simple example characteristically shows that a *discontinuous* function can be naturally regularized by a *continuous* function by *truncating* the *infinite* Fourier series by a *finite*  $L$  sum.  $L$  is here regarded as an infrared *regularization parameter*. The continuousness is indispensable for a wall-configuration with finite thickness or for a well-defined regularization. The meaning of  $1/L$  is the "thickness" of the walls or anti-walls of  $\theta_L'(x)$  at  $x = \epsilon\mathbf{Z}$ .<sup>4</sup> The thickness here is purely a *regularization* effect. See Fig.7.

With the above fact in mind, we propose here a *new regularization* in order to treat the singularity at  $z = \frac{1}{2} + \mathbf{Z}$  of the solutions in the previous section. First we know  $\Phi(z)$  and  $\Sigma(z) = F(z)\sigma'$  behave like a periodic  $\theta$ -function at some parameters limit ( the infinitely-thin wall limit).<sup>5</sup> Both satisfy the  $\Phi$ -properties in Sec.4. Imitating (25) with  $\epsilon = \frac{1}{2}$ , we take, as the regularized solution of (14), the following forms for  $\Phi(z)$  and  $\Sigma(z)$ .

$$\Phi_L(z) = v_0 \frac{4}{\pi} \sum_{l=0}^L \frac{d_l}{2l+1} \sin\{(2l+1)2\pi z\} \quad ,$$

---

<sup>4</sup> In the "wall region" around the origin  $|\frac{x}{\epsilon}| \ll 1$ , all  $L+1$  terms equally dominate in the RHS of (25) :  $\theta_L(x) \approx \frac{4}{\pi} \sum_{l=0}^L \frac{1}{2l+1} \{(2l+1)\pi \frac{x}{\epsilon}\} = \frac{4}{\epsilon}(L+1)x$ . Therefore the thickness  $w$  can be defined as :  $\frac{4}{\epsilon}(L+1)\frac{w}{2} = \frac{1}{2}$ , hence we have  $w = \frac{\epsilon}{4(L+1)}$ . The same thing can be said about all "wall-regions" around  $x \in \epsilon\mathbf{Z}$  and about all "anti-wall regions" around  $x \in \epsilon(2\mathbf{Z}+1)$ . It is well-known that, in these "wall and anti-wall regions" the truncated function  $\theta_L(x)$  most deviate from  $\theta(x)$  because the neglected terms (high-frequency modes) begin to equally contribute with low-frequency ones (Gibbs's phenomenon).

<sup>5</sup> The infinitely thin wall limit is given by  $\lambda v_0^2 \rightarrow +\infty$  (for a given  $v_0$  and an appropriately chosen  $\Lambda$ ).

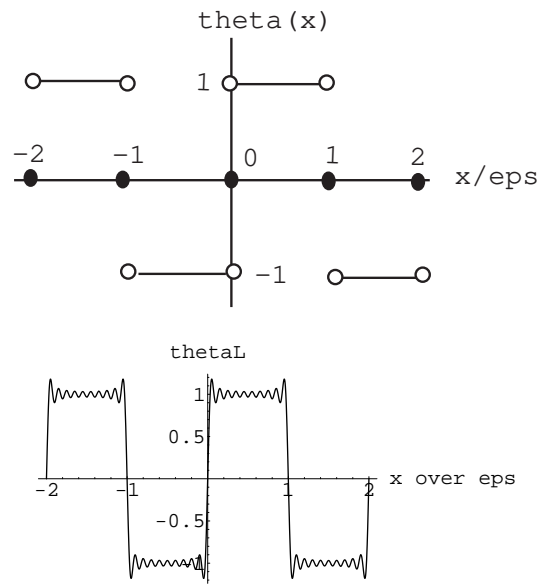


Fig.7 [Above] The periodic step function  $\theta(x)$  ((23) or (24)) and [Below] its regularized function  $\theta_{L=9}(x)$  ((25)). Horizontal axes:  $x/\epsilon$ .

$$\Sigma_L(z) = \omega \frac{4}{\pi} \sum_{l=0}^L \frac{c_l}{2l+1} \sin\{(2l+1)2\pi z\} \quad , \quad (26)$$

where  $c_l$ 's and  $d_l$ 's are some numbers to be determined appropriately and  $L$  is the new *regularization parameter* which should be taken sufficiently large. At present, the way to fix the coefficients,  $c_l$ 's and  $d_l$ 's, relies on a numerical method. (See App.B.1 for solving (14) numerically, and see App.B.2 for fixing the coefficients by the least square method.) As explained in App.C, the behavior of  $\{d_l\}$  and  $\{c_l\}$  has three "phases": i)  $2l+1 \ll 1/(4\pi w_{UV})$ , ii)  $2l+1 \approx 1/(4\pi w_{UV})$ , and iii)  $2l+1 \gg 1/(4\pi w_{UV})$ , where  $w_{UV}$  is the thickness around the UV regions ( $z \sim \mathbf{Z}$ ). The critical value  $l = L^*$  is given by the vacuum parameters:

$$\frac{L^*}{r_c} \sim \frac{1}{8\pi w_{UV}} \sim \sqrt{\lambda v_0^2} = m_H \quad , \quad (27)$$

where  $\sqrt{\lambda v_0^2}$  is identified as the (5 dim) Higgs mass  $m_H$  defined by  $m_H^2 \equiv \frac{1}{2}V''(v_0)$ . The (length) scale  $w_{UV}$  is an important quantity in the mass hierarchy problem.<sup>6</sup> These values  $L^*$  and  $w_{UV}$  are *independent of the regularization parameter*  $L$ . This point should be compared with the thickness appeared in  $\theta_L(x)$ . The condition for the *dimensional reduction*, from 5 dim to 4 dim, is given by

$$L^* \sim \frac{r_c}{8\pi w_{UV}} \gg 1 \quad . \quad (28)$$

In the present regularized solution (26), the *UV-IR symmetry* (i.e., symmetry w.r.t the axes  $z = \pm \frac{1}{4} + \mathbf{Z}$ ) holds. Therefore another width  $w_{IR}$  around the IR-regions ( $z \sim \frac{1}{2} + \mathbf{Z}$ ) is the same as  $w_{UV}$ .

$$w_{IR} = w_{UV} \quad . \quad (29)$$

$w_{IR}$  is protected against  $L$ (regulator) dependence, at least, taking the regularized form of (26). (This should be compared with the  $\theta_L(x)$  case, where  $w_{IR} = w_{UV} \sim L^{-1}$ .)

Both  $\Phi_L$  and  $\Sigma_L$  have the  $\theta_L$ -properties with  $\epsilon = \frac{1}{2}$ . We consider the case that  $L^*$  is large ( $L \gg L^* \gg 1$ ), that is, the solutions  $\Phi(z)$  and  $\Sigma(z)$  are near the  $\theta$ -function. The infinitely-thin wall limit ( $\theta$  or  $\delta$ -function distribution) corresponds to, in (26), the following case.

$$L \gg L^* \rightarrow \infty \quad , \quad d_l \rightarrow 1 \quad , \quad c_l \rightarrow 1 \quad \text{for all } l\text{'s} \quad . \quad (30)$$

---

<sup>6</sup> This new mass scale  $L^*/r_c$  corresponds to the parameter  $k$  in the original RS model[1, 2].

Taken into account the condition that the 5D *classical* Einstein equation works, that is, the new mass scale  $L^*/r_c$  should be much less than 5D Planck scale  $M$ , we should have the following relations between parameters.<sup>7</sup>

$$\frac{1}{r_c} \ll \frac{L^*}{r_c} \ll M \quad . \quad (31)$$

We regard the above three parameters,  $M$ (fundamental scale),  $r_c$ (compactification size) and  $L^*$ (wall-thickness parameter), as the *fundamental parameters* of the theory.

The numerical results of (26) are given in the next section. (See App.B for further detail of the calculation.) The solution (26) is the regularized solution of (14), not a true one. (How to improve (26) perturbatively, in order to approach a true solution, is proposed in Sec.8. In the practical and numerical point of view, the solution (26) is sufficiently close to the true solution.) It is, however, sufficient to claim the existence of the solution of (14) that has the wall-anti-wall (kink-anti-kink) configuration.

## 6 Final Numerical Result of $S^1/Z_2$ Compactification

In Fig.8,9 and 10, we plot three sample solutions of (26) corresponding to the following three vacua respectively. The configurations approach to the  $\theta$ -function in the order of Vac.1, 2 and 3.

$$\begin{aligned} \text{Vacuum 1} \quad & \lambda = 20.0(\text{input}) , \quad v_0 = 1.0(\text{input}) , \quad \Lambda = -1.88855 \\ & (\omega = 1.12207) , \quad L = 19(\text{input}); \quad w_{UV} \sim 8.9 \times 10^{-3} (L^* \sim 4.5). \end{aligned} \quad (32)$$

$$\begin{aligned} \text{Vacuum 2} \quad & \lambda = 40.0(\text{input}) , \quad v_0 = 1.0(\text{input}) , \quad \Lambda = -3.77762 \\ & (\omega = 1.58695) , \quad L = 19(\text{input}); \quad w_{UV} \sim 6.3 \times 10^{-3} (L^* \sim 6.3). \end{aligned} \quad (33)$$

$$\begin{aligned} \text{Vacuum 3} \quad & \lambda = 100.0(\text{input}) , \quad v_0 = 1.0(\text{input}) , \quad \Lambda = -9.4440537 \\ & (\omega = 2.5091903) , \quad L = 19(\text{input}); \quad w_{UV} \sim 4.0 \times 10^{-3} (L^* \sim 10.). \end{aligned} \quad (34)$$

Note that the values of the (5D) cosmological term,  $\Lambda$ , are very finely chosen so that the boundary conditions (17) and (18) are satisfied. All digits appearing are "significant figures". As the configuration approaches the  $\theta$ -function limit ( $m_H^2 = \lambda v_0^2 \rightarrow \infty$ ), the necessary number of digits increases.

---

<sup>7</sup> In (31) the  $r_c$ -dependence is explicitly written. The eq.(6), which was introduced purely for the notational simplicity, should be taken off and, instead,  $Mr_c \gg 1$  should be considered.



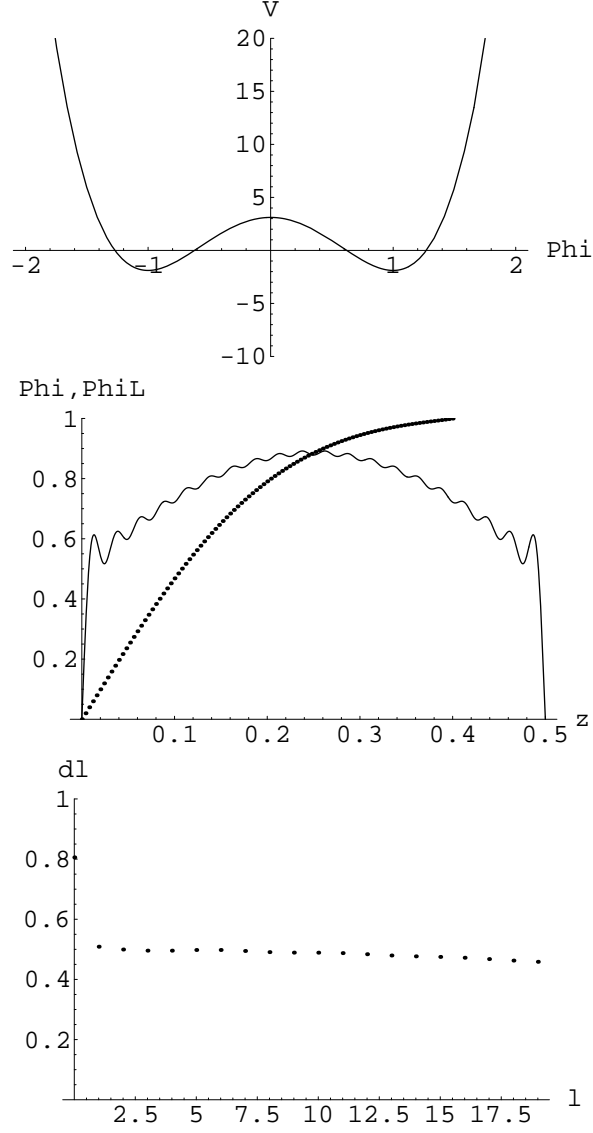


Fig.8 Vacuum 1  $(\lambda, v_0, \Lambda) = (20.0, 1.0, -1.88855)$ : [Top] Higgs Potential  $V(\Phi)$ , (1). The horizontal axis is  $\Phi$ . [Middle] Numerical result of  $\Phi(z)$  (dotted points,  $0 \leq z \leq 0.4$ ) for (14) and its least-square fit solution  $\Phi_L(z)$ , (26), ( $0 \leq z \leq 0.5$ ). The horizontal axis is  $z$ . [Bottom] The coefficients  $\{d_l ; l = 0, 1, \dots, L = 19\}$  of  $\Phi_L(z)$ . The horizontal axis is  $l$ .

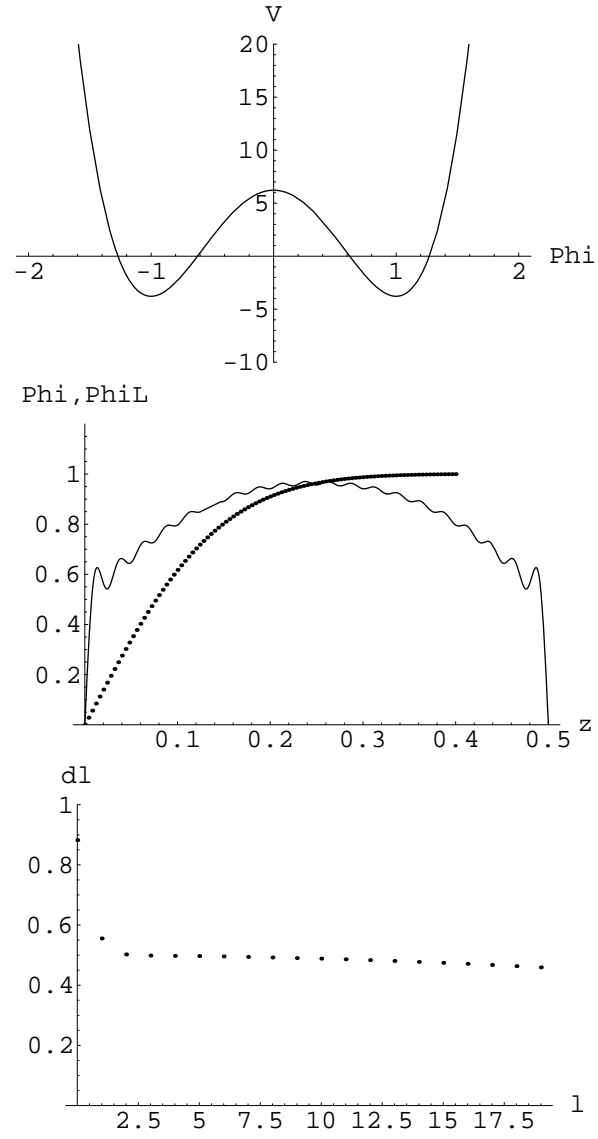


Fig.9 Vacuum 2  $(\lambda, v_0, \Lambda) = (40.0, 1.0, -3.77762)$ : same as the figure caption of Fig.8.

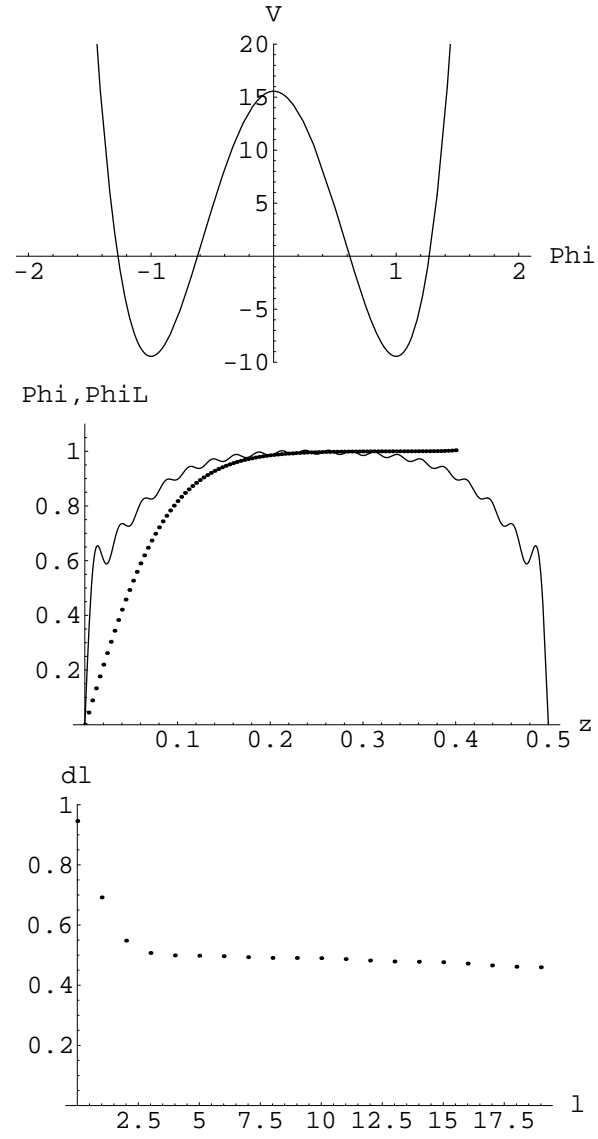


Fig.10 Vacuum 3  $(\lambda, v_0, \Lambda) = (100.0, 1.0, -9.4440537)$ : same as the figure caption of Fig.8.

(See also Vac.1w in App.A.) This shows the cosmological constant is, for a given  $\lambda$  and  $v_0$ , dynamically derived in the present framework. Note that  $\Lambda$  is directly related with the 4 dim cosmological constant[12].<sup>8</sup> In App.A, we give another result for Vac.1 with a different compactification coordinate.

The solutions of  $\Sigma(z)$  and  $\Sigma_L(z)$  are similar to  $\Phi(z)$  and  $\Phi_L(z)$ . In Fig.11,  $\Sigma(z)$  and  $\Sigma_L(z)$  are plotted for the case of Vacuum 3. For each vacuum,  $\Sigma(z)$  is always closer to the  $\theta$ -function limit than  $\Phi(z)$ .

The following items can be read from the above output data.

1. As the Higgs potential has deeper valleys, which corresponds to the case that the 5D Higgs mass ( $m_H = \sqrt{\lambda v_0^2}$ ) becomes larger,  $\Phi$  and  $\Sigma$  approach the  $\theta$ -function. All coefficients  $d_l$ 's and  $c_l$ 's are expected to approach 1 (the limit of (30)).
2. The wavy region, explained in (61), is not so clear in Vacuum 1-3, but can be seen in Vacuum 1w of App.A.

## 7 Properties of the Solution

### 7.1 Wall-Anti-Wall Configuration

In the previous section, the regularized (numerical) solutions for the wall-anti-wall configuration are given.  $S^1/Z_2$  compactification is just taking the segment  $[0, \frac{1}{2}]$  for the periodic coordinate  $z$  with periodicity 1. The derivative of  $\Phi_L(z)$  of Vacuum 3 (Fig.10) is plotted in Fig.12. Here we see the present approach surely gives the wall-anti-wall configuration. The walls appear at *both ends* of the extra axis, not at some middle points in the axis. The situation is the same as that in the lattice domain wall[18, 20]. We stress the points: 1) the anti-wall is realized by the present *IR regularization* where the discontinuity of  $\Phi(z)$  and  $\Sigma(z)$  at the singular points  $(\frac{1}{2} + \mathbf{Z})$  is avoided by *truncating the infinite Fourier series*; 2) the stability of the solution is guaranteed by the boundary conditions; 3) UV-IR symmetry is realized in the present form of the regularized solution.<sup>9</sup> We need not the radion field which was considered, for the stability, in [1] and was developed in [14].

---

<sup>8</sup> The cosmological constant problem was reviewed in [22]. One standard approach to the dynamical cosmological constant is the radiative correction. Such scenario was explicitly done, using the Coleman-Weinberg mechanism, in [23].

<sup>9</sup> In ref.[24], the wall-anti-wall configuration is considered in a modified RS-model and UV-IR symmetry is suggested.

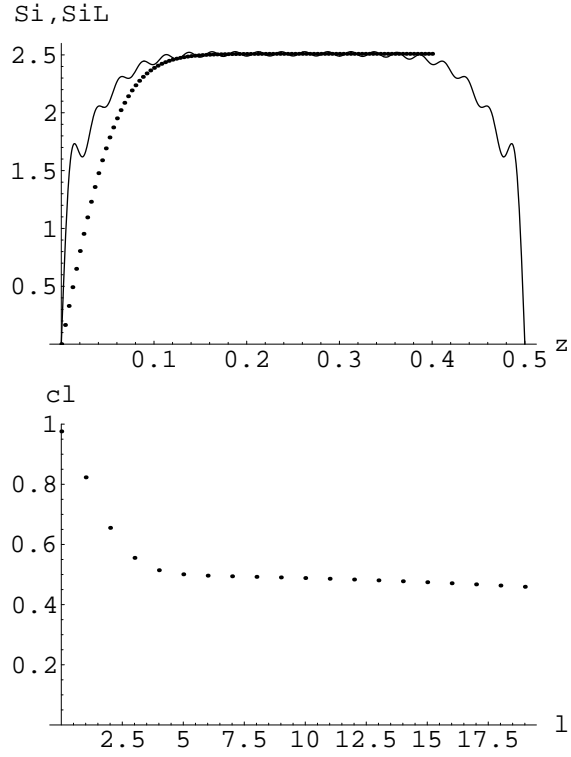


Fig.11 Vacuum 3: [Above] Numerical result of  $\Sigma(z)$  (dotted points,  $0 \leq z \leq 0.4$ ) and its least-square fit solution  $\Sigma_L(z)$ , (26), ( $0 \leq z \leq 0.5$ ).

The horizontal axis is  $z$ .

[Below] The coefficients  $\{c_l ; l = 0, 1, \dots, L = 19\}$  of  $\Sigma_L(z)$ . The horizontal axis is  $l$ .

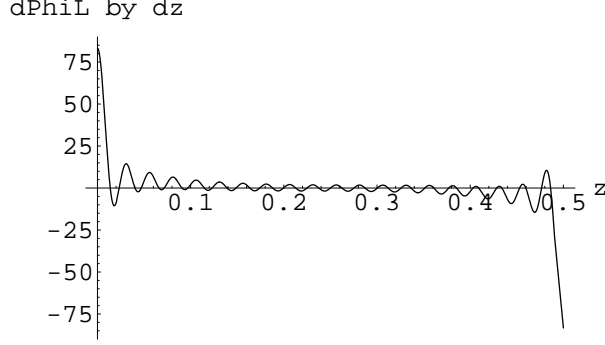


Fig.12 Plot of  $\frac{d\Phi_L(z)}{dz}$  where  $\Phi_L(z)$  is given in Fig.10(Vacuum 3). The horizontal axis is  $z$ .

(In the place of the radion field  $T^2(x)$ (eq.(13) of [1]), from eq.(7), the fixed function of  $z$ ,  $4/(1 - 4z^2)^2$ , appears in the present scenario. )

## 7.2 Brane Tensions at the Wall and the Anti-Wall

We make a remark on a comparative aspect between the wall and the anti-wall. Let us consider the " $\theta$ -function limit" (thin wall limit)  $m_H r_c = \sqrt{\lambda} v_0^2 r_c \sim L^* \gg 1$ . The behaviors of  $\Phi(z)$  and  $\Sigma(z) = \sigma' F(z)$  are considered to be the periodic step functions shown in Fig.13b and d. Correspondingly those of  $\Phi'$  and  $\Sigma'$  can be written as

$$\begin{aligned}\Phi' &= v_0 \sum_{n \in \mathbf{Z}} \left\{ \delta(z - n) - \delta\left(z - n - \frac{1}{2}\right) \right\} \quad , \\ \Sigma' &= \omega \sum_{n \in \mathbf{Z}} \left\{ \delta(z - n) - \delta\left(z - n - \frac{1}{2}\right) \right\} \quad .\end{aligned}\tag{35}$$

See Fig.13a and c. The "warp" factor  $\sigma(z)$  behaves as in Fig.13e. These behaviors should be compared with (8)-(10) of Ref.[1]. The parts of minus-delta-function in eq.(35) correspond to the anti-walls. Now we evaluate the integrand of the 5D action (1) near  $z \approx 0$ (Wall) and  $z \approx \pm \frac{1}{2}$ (Anti-Wall). Noting  $\partial_\mu \Phi = 0$ , we obtain

$$S = \int d^4x dz \frac{2e^{-4\sigma(z)}}{F(z)} \sqrt{-g} \left\{ -\frac{1}{2}(-2F\Sigma' + 5\Sigma^2) - \frac{1}{8}F(z)^2\Phi'^2 - \frac{\lambda}{4}(\Phi^2 - v_0^2)^2 - \Lambda \right\}$$

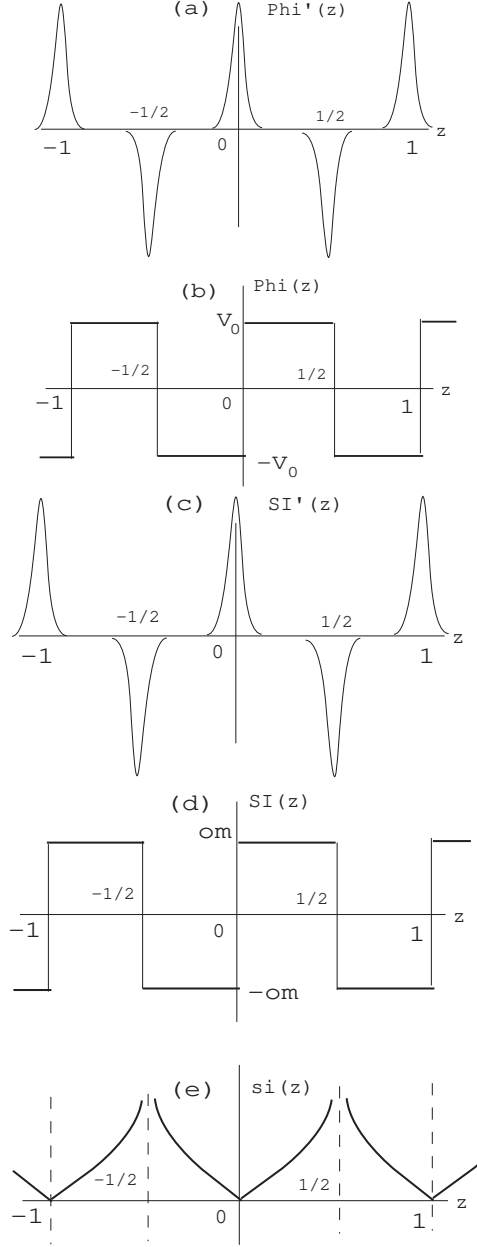


Fig.13 Behaviors at the thin-wall limit. Horizontal axis:  $z$ . (a)  $\Phi'(z)$ ; (b)  $\Phi(z)$ ; (c)  $\Sigma'(z)$ ; (d)  $\Sigma(z)$ ; (e)  $\sigma(z)$ . Especially, in Fig.13(e),  $\sigma \sim \omega z$  for  $z \sim +0$  and  $\sigma \sim (\omega/4) \ln(2/(1-2z)) + \text{const.}$  for  $z \sim (1/2) - 0$ .

$$\equiv \int d^4x dz L \quad , (36)$$

where we consider the general curved space  $g_{\mu\nu}(x)$  for the 4D world.

i)  $z \approx 0$

$$\begin{aligned} F &\sim 1 \quad , \quad |\Sigma| \sim \omega \quad , \quad e^{-4\sigma} \sim 1 \quad , \quad |\Phi| \sim v_0 \quad , \\ L &\sim \sqrt{-g} \left\{ (2\omega M^3 - \frac{1}{4} v_0^2 \frac{L^*}{r_c}) \delta(z) + \frac{4}{3} \Lambda \right\} \quad . \end{aligned} \quad (37)$$

The presence of  $\delta(z)$  term<sup>10</sup> shows the 3-brane is located at  $z = 0$ . The brane tension is given by

$$T_{UV} = 2\omega M^3 - \frac{1}{4} v_0^2 \frac{L^*}{r_c} \quad , \quad (38)$$

which is given by the value of  $\omega = \sqrt{-2\Lambda/3M^3}$  and  $v_0$ .  $T_{UV}$  is positive for the large value of  $\omega$ ,  $2\omega M^3 > \frac{1}{4} v_0^2 \frac{L^*}{r_c}$ .

ii)  $z \approx \frac{1}{2} - 0$

$$\begin{aligned} F &\sim 2(1-2z) \quad , \quad \Sigma \sim \omega \quad , \quad e^{-2\sigma} \sim \left(\frac{2}{1-2z}\right)^{-\omega/2} \quad , \quad \Phi \sim v_0 \quad , \\ L &\sim \frac{1}{2\omega} \sqrt{-g} \left\{ (-2\omega(1-2z)^\omega - \frac{v_0^2}{2} (1-2z)^{\omega+1}) \delta(z - \frac{1}{2}) + \frac{2}{3} \Lambda (1-2z)^{\omega-1} \right\} \\ &\quad \sim 0 \quad , (39) \end{aligned}$$

as far as  $\omega > 1/r_c$ .

iii)  $z \approx -\frac{1}{2} + 0$  (or  $+\frac{1}{2} + 0$ )

$$\begin{aligned} F &\sim 2(1+2z) \quad , \quad \Sigma \sim -\omega \quad , \quad e^{-2\sigma} \sim \left(\frac{1+2z}{2}\right)^{+\omega/2} \quad , \quad \Phi \sim -v_0 \quad , \\ L &\sim \frac{1}{2\omega} \sqrt{-g} \left\{ (-2\omega(1+2z)^\omega - \frac{v_0^2}{2} (1+2z)^{\omega+1}) \delta(z + \frac{1}{2}) + \frac{2}{3} \Lambda (1+2z)^{\omega-1} \right\} \\ &\quad \sim 0 \quad , (40) \end{aligned}$$

as far as  $\omega > 1/r_c$ . We see ii) and iii) are continuously connected at the Lagrangian *density* level. Note that singularities at  $z = \pm \frac{1}{2}$  are avoided by

---

<sup>10</sup> In (37), we have used relations:  $\delta(z) = \lim_{a \rightarrow +0} (1/\sqrt{2\pi}a) \exp\{-z^2/2a^2\}$ ,  $\delta(z)\delta(z) \sim \delta(z)/\sqrt{2\pi}a$ , where  $\sqrt{2\pi}a$  is regarded as the thickness of the wall,  $r_c/L^*$ .



the warp factors. The above result shows the anti-wall, in the thin wall limit, does not remain at the lagrangian density level. We may say the tension for the anti-wall is zero.

$$T_{IR} = 0 \quad . \quad (41)$$

This view is also confirmed, as far as the value of  $\omega$  is large, by the energy momentum tensor  $\sqrt{-G}T_{MN}$  where  $T_{MN}$  is given by the RHS of eq.(2).

$$\begin{aligned} \sqrt{-G}T_{\mu\nu} &= e^{-6\sigma} \sqrt{-g}g_{\mu\nu} \left( \frac{1}{4}F\Phi'^2 + \frac{2}{F}V \right) \\ \sim \begin{cases} \sqrt{-g}g_{\mu\nu} \left( \frac{1}{4}v_0^2\delta(z) + 2\Lambda \right) & z \sim 0 . \\ \frac{1}{2^{1.5\omega}} \sqrt{-g}g_{\mu\nu} \left\{ \frac{v_0^2}{2} (1-2z)^{1.5\omega+1} \delta(z - \frac{1}{2}) + \Lambda(1-2z)^{1.5\omega-1} \right\} \sim 0 & z \sim \frac{1}{2} - 0 . \\ \frac{1}{2^{1.5\omega}} \sqrt{-g}g_{\mu\nu} \left\{ \frac{v_0^2}{2} (1+2z)^{1.5\omega+1} \delta(z + \frac{1}{2}) + \Lambda(1+2z)^{1.5\omega-1} \right\} \sim 0 & z \sim -\frac{1}{2} + 0 . \end{cases} \\ \sqrt{-G}T_{zz} &= e^{-4\sigma} \sqrt{-g} \left( -\frac{1}{F}\Phi'^2 + \frac{8}{F^3}V \right) \\ \sim \begin{cases} \sqrt{-g}(-v_0^2\delta(z) + 8\Lambda) & z \sim 0 . \\ \frac{1}{2^\omega} \sqrt{-g} \left\{ -\frac{v_0^2}{2} (1-2z)^{\omega-1} \delta(z - \frac{1}{2}) + \Lambda(1-2z)^{\omega-3} \right\} \sim 0 & z \sim \frac{1}{2} - 0 . \\ \frac{1}{2^\omega} \sqrt{-g} \left\{ -\frac{v_0^2}{2} (1+2z)^{\omega-1} \delta(z + \frac{1}{2}) + \Lambda(1+2z)^{\omega-3} \right\} \sim 0 & z \sim -\frac{1}{2} + 0 . \end{cases} \end{aligned} \quad (42)$$

(We have assumed  $\omega > 3/r_c$  in the vanishing of  $\sqrt{-G}T_{zz}$  for the infrared cases. )

These results are accepted because we have changed only the infrared boundary condition of the one wall solution. The appreciable appearance of the anti-wall occurs only at the level of the equation of motion, not at the effective action level. On the wall the dynamics of the 4D world are operating, whereas it is suppressed (by the warp factor) on the anti-wall. From the situation in the 5D lattice simulation, it is quite interesting to see how the anti-wall works to provide the other chirality partner for the zero mode fermions bound on the wall.

### 7.3 Renormalization Group Flow

We make a comment from the viewpoint of the renormalization group in the spirit of AdS/CFT. The basic standpoint is to regard the 5 dim *classical* solution as a scaling trajectory [8, 9, 10] in the 4 dim *quantum* field theory. In the present case, it occurs near the horizons. As  $z \rightarrow (r_c/2) - 0$ , the asymptotic metric (22) says the scalar density "operator" of the 5 dim

cosmological term is approximated by

$$V(\Phi = v_0)\sqrt{-G} \approx \Lambda(1 - \frac{2z}{r_c})^{\omega r_c - 1} \sqrt{-g(x)} \equiv \bar{\Lambda}(z)\sqrt{-g(x)} \quad , \quad (43)$$

where the general curved space  $g_{\mu\nu}(x)$  is considered for the 4D world and  $\bar{\Lambda}(z)$  is a 4D scalar. We can interpret the meaning of  $w_{IR}$  of (29) as the (infrared) scaling parameter when the "scale"  $z$  approaches the singular point  $r_c/2$ .

$$\frac{r_c}{2} - z \sim w_{IR} \approx \frac{1}{8\pi} \frac{r_c}{L^*} \quad . \quad (44)$$

From above results, we obtain

$$\begin{aligned} \bar{\Lambda}(L^*) &\approx \Lambda(\frac{1}{4\pi L^*})^{\omega r_c - 1} \quad , \\ \beta_{|\bar{\Lambda}|} &\equiv \frac{\partial}{\partial(\ln L^*)} \ln |\bar{\Lambda}(L^*)| \approx -\omega r_c + 1 = -\sqrt{-\frac{2\Lambda}{3M^3}r_c} + 1 \quad . \end{aligned} \quad (45)$$

The last quantity corresponds to the (infrared) renormalization group ( $\beta$ -) function for  $|\bar{\Lambda}|$ . We know, from the result of Sec.6,  $-\Lambda$  is positive and is sufficiently large, hence we conclude  $\beta_{|\bar{\Lambda}|} < 0$ . The quantity  $|\bar{\Lambda}|$  is infrared asymptotic free, that is, it decreases as  $L^* \rightarrow \infty$ .<sup>11</sup>

## 8 Discussion and Conclusion

The regularized solution (26) cannot become a true one even when we take  $L = \infty$ , because one of its properties TL5=T5: symmetric with respect to  $z = \frac{1}{4}$ , does not match with the solution except the  $\theta$ -function limit. In order to approach a true solution, as done for the one-wall case [12], we must generalize the form of solution (26) by replacing the constants  $d_l$  and  $c_l$  by  $z$ -dependent functions  $d_l(z)$  and  $c_l(z)$  in the following forms.

$$\begin{aligned} d_l(z) &= \alpha_{l,0} + \frac{\alpha_{l,2}}{2!} \frac{[z^2]}{(L^*r_c)^2} + \frac{\alpha_{l,4}}{4!} \frac{[z^4]}{(L^*r_c)^4} + \dots \\ c_l(z) &= \beta_{l,0} + \frac{\beta_{l,2}}{2!} \frac{[z^2]}{(L^*r_c)^2} + \frac{\beta_{l,4}}{4!} \frac{[z^4]}{(L^*r_c)^4} + \dots \quad , \end{aligned} \quad (46)$$

---

<sup>11</sup> In the renormalizable model of 2 dim  $R^2$ -gravity, the same property of the cosmological constant is known[25]. In the brane world context, a similar result is obtained and analysed in a different treatment[26, 27, 28].

where  $[z^n]$  is the "periodic generalization" of  $z^n$  ( in the same way as  $F(z)$  in Sec.4). (Compare with eq.(30) of [12].) In the above we take only even powers of  $z$  in order to keep the odd function property ( P4 or TL4=TL4). Note that the above generalization breaks the UV-IR symmetry (T5=TL5). Therefore the present solution, (26) with above generalization (46), can be regarded as the perturbation around the UV-IR symmetry limit.

As for the key equations (26) and their generalization (46), we can understand them by a set of general properties. Let  $f(x)$  be a real function defined on  $x \in \mathbf{R} = (-\infty, \infty)$ . If  $f(x)$  satisfy the following properties:

**G1** Piecewise continuous everywhere.

**G2** Piecewise smooth everywhere.

**G3** Periodic with the periodicity of 1 ( $S^1$ -symmetry) :  $f(x) = f(x + 1)$ .

**G4** Odd function ( $Z_2$ -symmetry) :  $f(-x) = -f(x)$ . (Using the item G3, an important property :  $f(\mathbf{Z}) = 0$  is deduced.)

**G5** Symmetric with respect to  $x = \frac{1}{4}$  (UV-IR symmetry).

then, the general form can be written as

$$f(x) = \sum_{l=0}^{\infty} a_l \sin\{(2l+1)2\pi x\} \quad , \quad (47)$$

where  $\{a_l\}$  are constants. If we replace the infinite sum by the finite sum  $\sum_{l=0}^L$  for the regularization, the word "piecewise" in the items G1 and G2 can always be removed. As a "deformation" of (47), at the cost of the item G5 (UV-IR symmetry), we can generalize the constants  $\{a_l\}$  to

$$a_l(x) = \alpha_{l,0} + \frac{\alpha_{l,2}}{2!}[x^2] + \frac{\alpha_{l,4}}{4!}[x^4] + \cdots \quad . \quad (48)$$

This generalization produces UV $\leftrightarrow$ IR (Planck $\leftrightarrow$ TeV) asymmetry.

Since Hořava-Witten's paper[29],  $S^1/Z_2$  compactification ( $Z_2$  orbifold) becomes popular as a dimensional reduction procedure in the string inspired unified models. It gives essentially an wall at one end of the extra axis and the anti-wall at the other. The present infrared regularization serves as realizing this configuration.

## Acknowledgment

The author thanks G.W.Gibbons for stimulating discussions at the initial stage and for comments at some stages. He also thanks T.Tamaribuchi for the help in the numerical calculation and N.Ikeda for some discussions.

## Appendix A : Stereographic Compactification

Instead of the compact coordinate  $z$  defined by (5), we can take another one  $w$  defined as

$$My = \tan \pi \frac{w}{r_c} \quad , \quad -\frac{1}{2} < \frac{w}{r_c} < \frac{1}{2} \quad , \quad -\infty < My < \infty \quad . \quad (49)$$

See Fig.14. We take  $M = r_c = 1$ . The line element (4) is rewritten as

$$ds^2 = e^{-2\sigma(w)} \eta_{\mu\nu} dx^\mu dx^\nu + \frac{\pi^2}{\{\cos(\pi w)\}^4} dw^2 \quad ,$$

$$dy = \frac{\pi}{\{\cos(\pi w)\}^2} dw \quad . \quad (50)$$

$w = \pm \frac{1}{2}$  are the points of the coordinate singularity. The boundary condition is

$$\lim_{w \rightarrow \pm(\frac{1}{2}-0)} \Phi(w) \rightarrow \pm v_0 \quad , \quad v_0 > 0 \quad . \quad (51)$$

The Einstein equation (2) reduces to the same form as (14) but with a different  $F$ .

$$-\frac{3}{2} \left( \frac{d\sigma}{dw} \right)^2 F_1(w)^2 = -\frac{1}{8} F_1(w)^2 \left( \frac{d\Phi}{dw} \right)^2 + V \quad ,$$

$$\frac{3}{4} \frac{1}{F_1(w)} \frac{d}{dw} \left\{ \frac{d\sigma}{dw} F_1(w) \right\} = \frac{1}{4} \left( \frac{d\Phi}{dw} \right)^2 \quad ,$$

$$F_1(w) = \frac{2}{\pi} \{\cos(\pi w)\}^2 \quad . \quad (52)$$

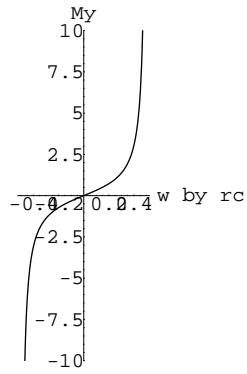


Fig.14 Relation between two coordinates,  $w$  (compact) and  $y$  (noncompact), (49). Vertical axis:  $My$ ; Horizontal axis:  $\frac{w}{r_c}$ .

Compared with the case using the coordinate  $z$ , the above equations are straightforward to the generalization from  $w \in (-\frac{1}{2}, \frac{1}{2})$  to  $w \in \mathbf{R} = (-\infty, \infty)$  because  $F_1(w)$  is periodic w.r.t.  $w \rightarrow w + 1$ . The properties of  $F_1(w)$  is the same as those of  $F(z)$  except a slightly better situation in the point F2: smooth everywhere. All procedures in the text are valid for the coordinate  $w$  just by replacing  $F(z)$  by  $F_1(w)$ .

In Fig.15, we give a sample result for Vacuum 1w ( $\lambda=20.0$ (input),  $v_0 = 1.0$ (input),  $\Lambda=-1.888810641$ ,  $\omega=1.122143972$ ). It should be compared with Vacuum 1 in the text. The shape of the Higgs potential  $V(\Phi)$  is almost same as that of Vacuum 1(Fig.8), but that of  $\Phi(z)$  is much closer to the  $\theta$ -function. ( In accordance with this, more digits are required for the appropriate value of the cosmological constant  $\Lambda$ . ) The "wavy" behavior (App.C) is recognized in the plot of  $\{d_l\}$ . The different choice of coordinate gives the different behaviors such as the sharpness of  $\Phi$  (or the value of  $w_{UV}$ ).

## Appendix B : Numerical Results in Sec.6

The numerical results of Sec.6, where the regularized solution (26) of the field equation (14) is given, are obtained as follow.

### Appendix B.1 : Numerical Solution by Runge-Kutta Method

First we can directly solve the coupled field equation (14) using the numerical method. In terms of  $\Phi(z)$  and  $\Sigma(z) \equiv F(z)\sigma'(z)$ , the field equation (14) can be written as

$$\begin{aligned} \frac{d\Phi}{dz} &= \pm \frac{\sqrt{2}}{F(z)} \{6\Sigma^2 + \lambda(\Phi^2 - v_0^2)^2 + 4\Lambda\}^{\frac{1}{2}} \quad , \\ \frac{d\Sigma}{dz} &= \frac{2}{3F(z)} \{6\Sigma^2 + \lambda(\Phi^2 - v_0^2)^2 + 4\Lambda\} \quad , \end{aligned} \quad (53)$$

where  $\lambda, v_0$  and  $\Lambda$  are the vacuum parameters.  $F(z)$  is  $(1 - 4z^2)$  in the text (Sec.4), and  $(2/\pi)(\cos \pi z)^2$  in App.A. Due to the periodicity and the odd function property, we may focus on an region  $[0, \frac{1}{2})$  of  $z$  and may take only the  $+$  sign in the first equation above. The above coupled differential equation about  $(\Phi(z), \Sigma(z))$  can be numerically solved, for a given

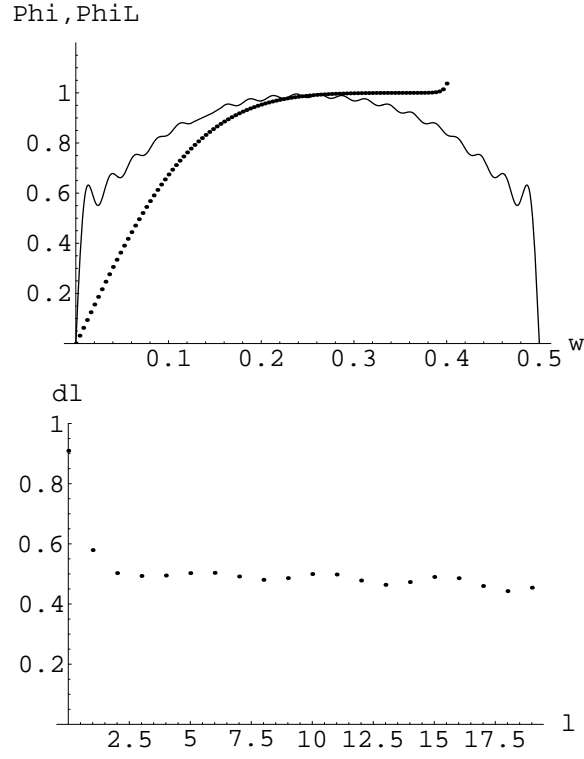


Fig.15 Vacuum 1w  $(\lambda, v_0, \Lambda) = (20.0, 1.0, -1.888810641)$  : [Above]  
 Numerical result of  $\Phi(w)$  (dotted points,  $0 \leq w \leq 0.4$ ) and its best fit  
 approximate solution  $\Phi_L(w)$ , (26). Horizontal axis is  $w$ .  
 [Below] The coefficients  $\{d_l ; l = 0, 1, \dots, L = 19\}$  of  $\Phi_L(w)$ .

vacuum parameters  $(\lambda, v_0, \Lambda)$ , by the Runge-Kutta method. As for the boundary condition we cannot take (17) and (18):  $\lim_{z \rightarrow \frac{1}{2}-0} \Phi(z) \rightarrow v_0$  and  $\lim_{z \rightarrow \frac{1}{2}-0} \Sigma(z) = \omega = \sqrt{-\frac{2\Lambda}{3}}$ , because of the singularity at  $z = \frac{1}{2}$ . Instead of this condition in the IR (or asymptotic) region, we take

$$\Phi(z=0) = \Sigma(z=0) = 0 \quad . \quad (54)$$

This is the condition in the UV (or non-asymptotic) region. Note that the above one is the *necessary condition* when we take the boundary condition (9) or the odd function property of  $\Phi(z)$  and  $\Sigma(z)$  (see sentences around (20)). We take the following procedure to have a reliable result.

1. Taking the above boundary condition, we numerically compute (53) for the region  $[0, 0.4]$ . Here we stop the calculation a little before the singularity point  $z = 0.5$ .
2. There appear three patterns in the calculational results: a) They diverge before  $z$  reaches 0.4; b) They become imaginary before  $z$  reaches 0.4; c) Calculation lasts to  $z = 0.4$  and all values converge to finite ones. Which pattern appears depends on the choice of the vacuum parameters  $(\lambda, v_0, \Lambda)$ .
3. Among the results of pattern c), we pick up the best one near to the "practical" boundary condition:  $\lim_{z \rightarrow 0.4} \Phi(z) \rightarrow v_0$  and  $\lim_{z \rightarrow 0.4} \Sigma(z) \rightarrow \omega = \sqrt{-2\Lambda/3}$ . Generally, for a given  $(\lambda, v_0)$ (input), the calculational value  $\Phi$  or  $\Sigma$  tends to be suppressed (or get imaginary) when  $|\Lambda|$  increases, while it tends to increase (or diverge) when  $|\Lambda|$  decreases. The width of the wall (or the initial slope) can be controlled by  $\lambda v_0^2$ . After trying the calculation, with 20-50 values of  $\Lambda$ , for one input  $(\lambda, v_0)$ , we can always obtain a satisfactory solution. This says that the boundary condition (54) and the suitable choice of  $\Lambda$  realize the original boundary condition (9).
4. For the numerically inaccessible region  $(0.4, 0.5)$ , we put the asymptotic values  $v_0$  for  $\Phi$  and  $\sqrt{-2\Lambda/3}$  for  $\Sigma$  by hand. Note that this region is the asymptotic region, therefore it should be dynamically simple although numerically difficult due to the infrared singularity.

Some sample output data are given in the text ( $F(z) = 1 - 4z^2$ ) for several cases:  $(\lambda, v_0, \Lambda)$



$= (20.0, 1.0, -1.88855)$  [Fig.8],  $(40.0, 1.0, -3.77762)$  [Fig.9],  $(100.0, 1.0, -9.4440537)$  [Fig.10,11]. Another one is given in App.A ( $F(z) = (2/\pi)(\cos \pi z)^2$ ) for  $(\lambda, v_0, \Lambda) = (20.0, 1.0, -1.888810641)$  [Fig.15].

In ref.[30], using the y-coordinate (4), some quantities  $(\sigma'(y), \Phi(y), \hat{R}, \text{etc})$  are obtained both analytically and numerically.

## Appendix B.2 : Least Square Fitting

We fit the solution obtained in the previous subsection by the proposed 0-th order formula (26).  $L$  should be taken appropriately large. The critical value  $L^*$ , explained in App.C, can be roughly obtained by

$$\frac{L^*}{r_c} \sim \sqrt{\lambda v_0^2} \quad . \quad (55)$$

Next we fix the coefficients  $d'$ 's and  $c'$ 's of (26). A standard way is to minimize the following quantity (Least square method).

$$\begin{aligned} I(d_0, d_1, \dots, d_L) &= \int_0^{1/2} (\Phi(z) - \Phi_L(z))^2 dz \quad , \quad \delta I = 0 \quad , \\ J(c_0, c_1, \dots, c_L) &= \int_0^{1/2} (\Sigma(z) - \Sigma_L(z))^2 dz \quad , \quad \delta J = 0 \quad , \end{aligned} \quad (56)$$

where  $\Phi(z)$  and  $\Sigma(z)$  are regarded as the exact solution. Solving this equation, we obtain

$$\frac{v_0}{\pi} \frac{d_l}{2l+1} = \int_0^{1/2} \Phi(z) \sin\{(2l+1)2\pi z\} dz \quad , \quad (57)$$

$$\frac{\omega}{\pi} \frac{c_l}{2l+1} = \int_0^{1/2} \Sigma(z) \sin\{(2l+1)2\pi z\} dz \quad , \quad . \quad (58)$$

The right hand side of the above equations can be numerically evaluated using the numerical results of  $\Phi(z)$  and  $\Sigma(z)$  in the previous subsection. The samples of  $\{d_l\}$  are given in Fig.8-10 and Fig.15, and  $\{c_l\}$  are in Fig.11.

## Appendix C : Trapezium Model Solution

As a simplified model of the solution of (14) or (53), we can take the following simplified model. See Fig.16.

$$\Phi(z) = \begin{cases} \frac{v_0}{2w} z & \text{when } 0 \leq z \leq 2w \\ v_0 & \text{when } 2w < z \leq \frac{1}{2} \end{cases} \quad (59)$$

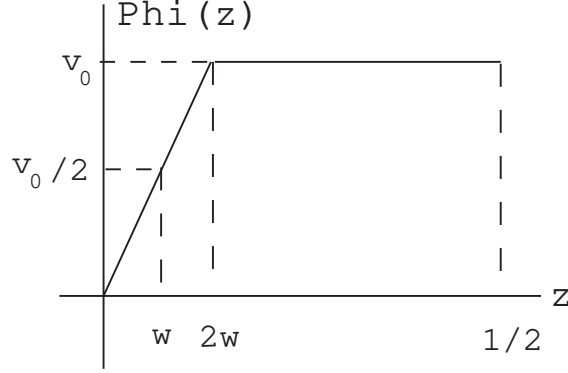


Fig.16 The trapezium model solution (59). The horizontal axis is  $z$ , and the vertical one is  $\Phi(z)$ .

We can qualitatively understand the behavior of the coefficients  $\{d_l\}$  appearing in the output data in Sec.6 and App.A. Using the formula (58),  $d_l$  is obtained as

$$d_l = \frac{1}{2} \left\{ \frac{\sin\{(2l+1)4\pi w\}}{(2l+1)4\pi w} + 1 \right\} \quad , \quad l = 0, 1, \dots, L \quad . \quad (60)$$

Generally three "phases" appear depending upon some regions of  $l$ .

$$\begin{aligned} i) \quad 0 < (2l+1)4\pi w \ll 1 & : \quad d_l \approx 1 - \frac{4}{3}\pi^2 w^2 (2l+1)^2 \text{ (parabolic)} \\ ii) \quad (2l+1)4\pi w \approx 1 & : \quad \text{wavy region} \\ iii) \quad (2l+1)4\pi w \gg 1 & : \quad d_l \approx \frac{1}{2} \text{ (constant)} \end{aligned} \quad (61)$$

The critical value of  $l \equiv L^*$  is given by

$$L^* \approx \frac{1}{8\pi w} \quad , \quad (62)$$

which is independent of the regularization parameter  $L$ . In Fig.17 and 18, we plot the above result for  $(L, w)=(19, 0.15)$  and  $(L, w)=(19, 0.05)$  respectively.

## References

- [1] L.Randall and R.Sundrum,  
Phys.Rev.Lett.**83**(1999)3370, hep-ph/9905221

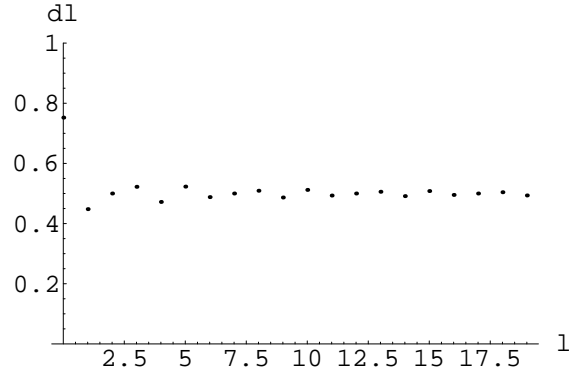


Fig.17 The plot of  $\{d_l\}$  for the trapezium model (60).  $(L, w)=(19, 0.15)$ .  
The horizontal axis :  $l$ ;  $l=0, 1, \dots, 19$ .

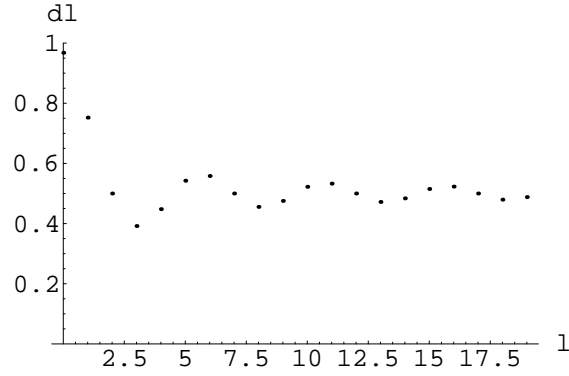


Fig.18 The plot of  $\{d_l\}$  for the trapezium model (60).  $(L, w)=(19, 0.05)$ .  
Axes are the same as in Fig.14.

- [2] L.Randall and R.Sundrum,  
Phys.Rev.Lett.**83**(1999)4690,hep-th/9906064
- [3] J.L. Hewett, Talk at XXXth Int. Conf. on High Energy Physics  
(ICHEP2000), Jul.27-Aug.2, 2000, Osaka, Japan, "Phenomenology of  
extra dimensions"
- [4] R. Kallosh and A. Linde, JHEP**0002**(2000)005, hep-th/0001071
- [5] G.W. Gibbons and N.D. Lambert, Phys.Lett.**B488**(2000)90, hep-  
th/0003197.
- [6] N.Arkani-Hamed, S.Dimopoulos and  
G.Dvali,Phys.Lett.**B429**(1998)263; Phys.Rev.**D59**(1999)086004
- [7] I.Antoniadis, N.Arkani-Hamed, S.Dimopoulos and G.Dvali,  
Phys.Lett.**B436**(1998)257
- [8] J.Maldacena, Adv.Theor.Math.Phys.**2**(1998)231,hep-th/9711200
- [9] E. Witten, Adv.Theor.Math.Phys.**2**(1998)253
- [10] J.de Boer,E.Verlinde and H.Verlinde, JHEP**0008**(2000) 003, hep-  
th/9912012
- [11] C.Csáki,J.Erlich,T.J.Hollowood and Y.Shirman,  
Nucl.Phys.**B581**(2000)309, hep-th/0001033.
- [12] S.Ichinose,Class.Quant.Grav.**18**(2001)421,hep-th/0003275
- [13] S.Ichinose,Proc. of the 30th Int. Conf. on High Energy Physics  
(ICHEP2000). (Jul.27-Aug.2,2000,Osaka Int. House,Osaka,Japan.) "An  
Exact Solution of the Randall-Sundrum Model and the Mass Hierarchy  
Problem"
- [14] W.D.Goldberger and M.B.Wise, Phys.Rev.Lett.**83**(1999)4922,hep-  
ph/9907447
- [15] D.B.Kaplan,Phys.Lett.**B288**(1992)342
- [16] K.Jansen,Phys.Lett.**B288**(1992)348
- [17] C.G.Callan and J.A.Harvey,Nucl.Phys.**B250**(1985)427

- [18] Y.Shamir,Nucl.Phys.**B406**(1993)90
- [19] M.Creutz and I.Horváth,Phys.Rev.**D50**(1994)2297
- [20] P.M.Vranas,Phys.Rev.**D57**(1998)1415, hep-lat/9705023
- [21] T.Blum et al,CU-TP-980,BNL-HET-00/20,RBRC-114,hep-lat/0007038,"Quenched Lattice QCD with Domain Wall Fermions and the Chiral Limit"
- [22] S.Weinberg,Rev.Mod.Phys.**61**(1989)1
- [23] S.Ichinose,Nucl.Phys.**B231**(1984)335
- [24] A.Gorsky and K.Selivanov,Phys.Lett.**B485**(2000)271,hep-th/0005066
- [25] S.Ichinose,Nucl.Phys.**B457**(1995)688
- [26] S.-H.Tye and I.Wasserman, Phys.Rev.Lett.**86**(2001)1682, hep-th/0006068.
- [27] A.Krause,hep-th/0006226,"A Small Cosmological Constant,Grand Unification and Warped Geometry"
- [28] A.Krause,hep-th/0007233,"A Small Cosmological Constant and Back-reaction of Non-Finetuned Parameters"
- [29] P.Hořava and E.Witten, Nucl.Phys.**B460**(1996)506,hep-th/9510209
- [30] S.Ichinose, Univ.of Shizuoka preprint,US-01-03,hep-th/0107254, "Some Properties of Domain Wall Solution in the Randall-Sundrum Model"